

Optimisation of High Efficiency $\text{Al}_x\text{Ga}_{1-x}\text{As}$ MQW Solar Cells

J.P.Connolly, K.W.J.Barnham, J.Nelson, P. Griffin, G. Haarpaintner

Blackett Laboratory, Imperial College of Science, Technology and Medicine, London SW7 2BZ

C.Roberts

IRC for Semiconductor Materials, Imperial College of Science, Technology and Medicine, London SW7 2BZ

M.Pate, J.S.Roberts

EPSRC III-V Facility, University of Sheffield, Sheffield S1 3JD

The $\text{GaAs}/\text{Al}_x\text{Ga}_{1-x}\text{As}$ materials system is well suited to multi-bandgap applications such as the multiple quantum well solar cell. GaAs quantum wells are inserted in the undoped $\text{Al}_x\text{Ga}_{1-x}\text{As}$ active region of a $p - i - n$ structure to extend the absorption range while retaining a higher open circuit voltage than would be provided by a cell made of the well material alone. Unfortunately aluminium gallium arsenide ($\text{Al}_x\text{Ga}_{1-x}\text{As}$) suffers from poor transport characteristics due to DX centres and oxygen contamination during growth, which degrade the spectral response. We investigate three mechanisms for improving the spectral response of the MQW solar cell while an experimental study of the open circuit voltage examines the voltage enhancement. An optimised structure for a high efficiency $\text{GaAs}/\text{Al}_x\text{Ga}_{1-x}\text{As}$ solar cell is proposed.

1 Introduction

One of the best materials for single band-gap solar cells is GaAs. Single crystal GaAs has high minority carrier mobility and a direct bandgap close to the optimum for single band-gap solar cells. A novel high efficiency design, the quantum well solar cell (QWSC), is illustrated in figure 1. The multiple quantum wells (MQWs) in the depletion region extend the absorption range below the barrier band-gap. Comparison of $\text{Al}_{0.3}\text{Ga}_{0.7}\text{As}$

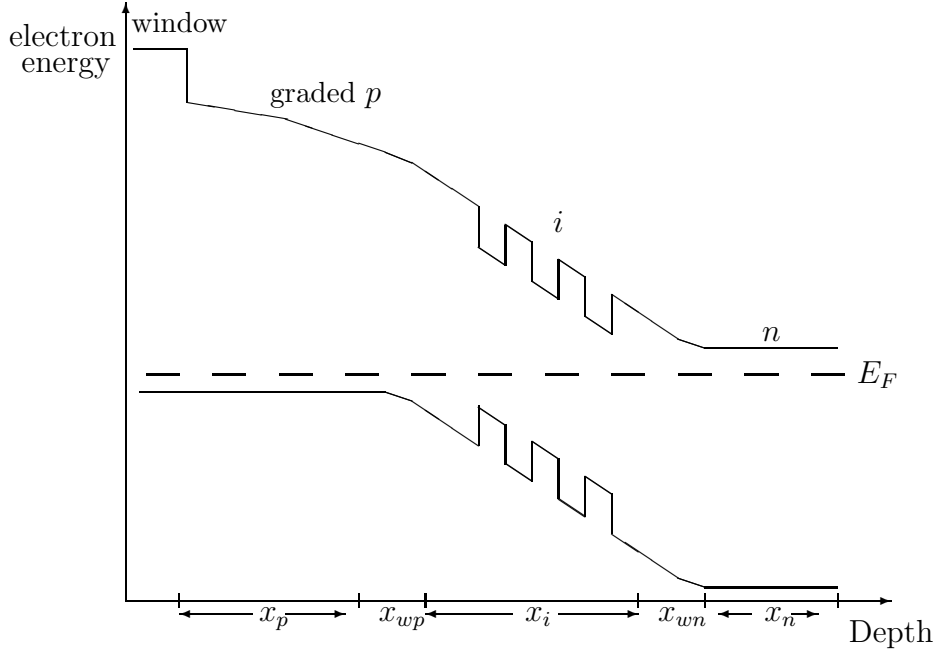


Fig. 1. QWSC band diagramme. The structure is a $p - i - n$ photodiode design with quantum wells in the intrinsic region. A high band-gap $\text{Al}_x\text{Ga}_{1-x}\text{As}$ window is grown on the top surface to reduce surface recombination.

devices with and without quantum wells has shown that the J_{sc} is more than doubled in samples with 50 MQWs. Furthermore, the V_{oc} provided by QWSCs is higher than would be expected from a cell with the quantum well effective bandgap. This provides the potential for a QWSC cell with a higher fundamental efficiency limit than a single band-gap cell. In order to test this idea in the $\text{GaAs}/\text{Al}_x\text{Ga}_{1-x}\text{As}$ materials system the short circuit current (J_{sc}) must be increased further. This can be achieved through improved growth and cell design.

Bulk $\text{Al}_x\text{Ga}_{1-x}\text{As}$ cells generally suffer from a relatively poor photon to photocurrent conversion efficiency (quantum efficiency or QE). Part of this poor performance stems from a DX centre associated with the proximity in energy of the Γ , X and L band gaps in energy at approximately 35% aluminium (Al) [11]. Oxygen contamination from the Al sources during growth contributes further to decreasing minority carrier lifetimes with increasing Al fraction X .

Three methods of optimising the QE are described. The first is investigated in [9] and consists of thinning the p layer thickness. This improves minority carrier collection by

reducing the mean distance carriers must diffuse before reaching the junction. Moreover, the absorptivity of the *p* layer is reduced, allowing more light to reach the efficient intrinsic (*i*) region. However, the J_{sc} current enhancement is offset by increased *p* layer series resistance.

The second method consists of linearly grading X in the *p* layer so that the bandgap decreases with depth. This also reduces the *p* layer absorptivity, and enhances the *i* region photocurrent. Furthermore, minority carriers generated in the *p* are swept towards the junction with the intrinsic region by the band-gap gradient. This only affects the QE at energies above the $Al_xGa_{1-x}As$ band-gap. At very high Al content, carrier collection efficiency tends to decrease because of a deterioration in material quality.

The third improvement consists of etching off the GaAs substrate and coating the back of the cell with a mirror. This is very effective for a QWSC design because the wells absorb a relatively small fraction of the incident light but convert it into current with nearly 100% efficiency.

The following discussion outlines the voltage study described in [5]. Thinner *p* regions are described in [9] while the present work mainly investigates samples with graded layers and mirrors. Experimental and modelling results incorporating these methods are presented, with particular regard to QE enhancement in samples with graded *p* layers and mirror backed samples. The model is used to design an optimised structure for a 50 quantum well QWSC.

2 Voltage

Measurements in [5] have shown that the QWSC V_{oc} as a function of effective band-gap is higher than expected from detailed balance arguments. This has been seen in the GaAs/ $Al_xGa_{1-x}As$ indium gallium arsenide / indium phosphide and also the indium gallium phosphide / gallium arsenide materials systems. Photoluminescence and photocurrent studies of $Al_xGa_{1-x}As$ samples presented in [12] indicate that the quasi-Fermi level separation in the wells is also greater than expected. This phenomenon is not fully understood but may be due to the high thermal escape efficiencies observed at room temperature.

The observed voltage in a ungraded QWSC with 20% Al fraction in the barrier X_{barr} was 1% higher than expected for a cell with the well bandgap. Similar voltage enhancements in cells with higher Al fraction were 7% with a $X_{barr}=30\%$ and 11% with $X_{barr}=40\%$. However, V_{oc} optimisation is limited by the decreasing QE at high X_{barr} .

3 Theory

3.1 Quantum Efficiency

The QE model differs from previous work by [9] and [7] by considering inhomogeneous material with position dependent materials parameters. We compare the modelled QE with experimental data for graded p layer devices. The QE of the cell is calculated by solving minority carrier transport equations at room temperature. The calculation of photocurrent from doped layers applies equally to p and n regions, with appropriate materials parameters. The n region contribution is small because little light with sufficient energy reaches it. For this region, the following discussion concentrates on photocurrent contributions from the p and i layers. Under illuminated conditions, the excess minority carrier generation rate as a function of depth x from the surface of the p layer is given by

$$G(x, \lambda) = F(\lambda)(1 - R(\lambda))\alpha(x, \lambda) \times \exp(-\int_0^x [\alpha(x, \lambda)] dx) \quad (1)$$

where $R(\lambda)$ is the surface reflectivity, $\alpha(x, \lambda)$ is the absorption coefficient and $F(\lambda)$ is the incident photon flux. Current and continuity equations determine the excess minority carrier concentration $n(x)$. Since the cell operates in the low injection limit we use the Einstein relationship between mobility and diffusion constant. The excess carrier concentration $n(x)$ in the p layer can then be found by solving

$$\frac{d^2n}{dx^2} + \frac{qE(x)}{k_B T} \frac{dn}{dx} - \frac{n}{L_n(x)^2} + \frac{G(x, \lambda)}{D_n(x)} = 0 \quad (2)$$

L_n and D_n are the electron diffusion length and diffusion constant respectively. $E(x)$ is the depth dependent effective electric field due to the bandgap gradient. The expressions for the band-gap are due to [3] (direct gap) and [8] (indirect). The smaller contributions to the effective field from the bulk photovoltaic effect, the mobility gradient and the Dember potential are neglected.

The boundary condition at the surface is determined by matching the drift and diffusion currents to the surface recombination current. For the p layer, this takes the form

$$\frac{qDE(x)}{KT} n(x) + qD_n(x) \nabla n(x) = S_n n(x) \quad (3)$$

at $x = 0$

where S_n is the minority electron surface recombination velocity. The second boundary condition in the depletion approximation is that of zero excess minority carrier concentration at the edge of the depletion region for p respectively:

$$n(x_{wp}) = 0 \quad (4)$$

Equation 2 has an analytical solution for ungraded samples with constant transport parameters in the doped layers. For graded samples with depth dependent transport characteristics, a standard numerical method is used. The photocurrent $J_p(\lambda)$ from the p is given by the diffusion current at the depletion edge

$$J_p(\lambda) = qD_n \nabla n(x_{wp}) \quad (5)$$

where x_{wp} is the position of the p depletion edge. This expression assumes zero excess minority carrier concentration at the edge of the junction within the depletion approximation.

The validity of the this approximation on the minority carrier gradient at the edge of the junction was verified by analytically calculating the photocurrent in the light at x_{wp} for an ungraded sample with a high current density. This was compared with the numerical result for the same device. The largest error was was of the order of 0.1% for a GaAs cell in the resulting photocurrent from the p layer.

Assuming 100% collection efficiency, the current $J_i(\lambda)$ from the i region is calculated from the integral of the generation rate over the depleted regions

$$J_i(\lambda) = q \int_{x_p - x_{wp}}^{x_p + X_i + x_{wn}} [G(x, \lambda)] dx \quad (6)$$

The short circuit current is then the sum of the contributions from the three regions

$$J_{sc}(\lambda) = J_p(\lambda) + J_i(\lambda) + J_n(\lambda) \quad (7)$$

where the n region photocurrent J_n is calculated in a similar fashion to J_p . The QE is defined in terms of J_{sc} and the incident flux

$$QE(\lambda) = \left[\frac{J_{sc}(\lambda)}{qF(\lambda)} \right] \quad (8)$$

3.2 Mirrors

The normal incidence mirror model treats the cell as a cavity with uniform light intensity for a given wavelength. The refractive index is an average over the structure.

The light intensity in the QWSC is calculated as a function of wavelength by summing electric field amplitudes due to successive reflections. The wavelength dependence of the front and back surface reflectivities is neglected. A wavelength independent back surface reflection phase change is included. The mean light intensity in the cell is given by the squared modulus of the total electric field amplitude. The QE enhancement above the well is neglected because of the low levels of light reaching the back mirror at these wavelengths.

4 Modelling Method

4.1 QE model Parameters

The main model parameters are the reflectivity, the absorption coefficient, S_n , D_n and L_n . Reflectivities were measured on a separate set of large area calibration samples described in section 5. An average reflectivity is used in the modelling since the measured data vary by no more than a few percent. Modelling of the absorption coefficient is described in [9]. The surface recombination velocity S_n is very dependent on sample growth and processing and is essentially used as a fitting parameter at wavelengths below 400nm.

L_n is also sensitive to growth and processing. A wide range of values exist in the literature ([1], citehamaker85) and reliable published data can only be found for X compositions below approximately 40%. A number of simpler ungraded QWSC structures were grown at different values of X in order to increase our knowledge of L_n . The following method was used to extract values of this parameter.

Inspection of the analytical solution to equation 2 and equation 5 shows that the expression for the QE is independent of D_n if D_n is a constant. The only free parameters in this case are S_n and L_n . S_n mainly influences the QE at short wavelengths whereas L_n affects longer wavelengths. The ungraded p layer QE can therefore be modelled in terms of S_n at short wavelengths and L_n at long wavelengths.

Fitting QE measurements of $p - i - n$ and QWSC samples without grades have enabled us to extract values of the diffusion length for X ranging from 20% to 47%. Since we have no samples outside this range, we use the parameterisation in [6] for X compositions above 47%.

We use the values of L_n described above to model graded QWSC samples. This assumes that the X dependence of the diffusion length in the graded p is similar to the behaviour observed in separate ungraded structures with different X compositions. In graded samples, however, D_n is no longer a constant, and has a significant effect on the QE.

Inspection of equations 2 and 8 shows that for a graded sample the QE depends on the gradient of the diffusion constant with X composition $\nabla_X D_n$ but not on the its magnitude

of D_n . The graded p layer QE can therefore be modelled in terms of $\nabla_X D_n$. In the absence of detailed D_n measurements, we assume a constant gradient $\nabla_X D_n$ between the two Al fractions for each p layer and use this constant as the main fitting parameter.

4.2 Mirror Parameters

Modelling the mirrors involves three parameters. We find that for low front surface reflectivities the back surface reflectivity mainly determines the level of QE increase in the wells. The amplitude of Fabry-Perot oscillations is set by the front surface. The phase change upon reflection from the back surface is a poorly understood quantity, but partly determines the position of Fabry-Perot peaks.

5 Samples

The MBE samples were grown on a V80H Vacuum Generators machine. The growth temperature was at 630°C. Temperature monitoring was carried out using an optical pyrometer backed up by a substrate thermocouple and RHEED observation of oxygen desorption from the surface at 590°C. The flux ratios (As:Ga 10:1) were measured with a beam monitoring ion gauge.

A series of ungraded 30 well QWSCs and control $p - i - n$ structures were grown by MBE at nominal Al fractions of 20%, 30% and 40%. These samples have $0.03\mu\text{m}$ windows grown at $X=67\%$. The Al fraction is subject to increasing uncertainty up to about $X=50\%$ because of Ga source flux fluctuations. The controls are identical in every respect except that the well material is replaced by $\text{Al}_x\text{Ga}_{1-x}\text{As}$ with the barrier Al fraction. A $\text{Al}_{0.2}\text{Ga}_{0.8}\text{As}$ double heterostructure $p - i - n$ was also grown.

A set of three graded QWSCs was grown on the same MBE machine. The X compositions were calculated from the photocurrent spectra. The Al fraction in the graded p regions varies from $X=44\%$ at the front surface to $X=22\%$ at the p - i interface in sample U4033. Analogous grades in samples U4034 and U4035 ranged from 67% to 34% and 67% to 47% respectively.

MOVPE growth details are given in [10]. Sample QT468a is a 30 well ungraded QWSC with a 80% $0.02\mu\text{m}$ $\text{Al}_x\text{Ga}_{1-x}\text{As}$ window.

The samples were processed to circular 1mm gold ring contact photodiode devices with a circular $600\mu\text{m}$ optical window. The devices are mounted on TO5 headers.

The anti-reflection (AR) coating consists of 75nm of SiN. Large area pieces of wafer from each sample were AR coated to allow reflectivity measurements to be carried out.

Coating the back of a device with a mirror is achieved by etching the substrate down to the n layer, which acts as an etch-stop. A metallic mirror is then evaporated directly onto

Sample	Type	Modelled p Al fraction (%)	Diffusion Length (μm)	S_n cm^2/s
U2027	mqw	22	0.075	10^{-5}
U2028*	pin DHet	22	0.075	10^{-5}
U4036	pin	22	0.075	10^{-5}
U2029	mqw	35	0.06	10^{-4}
U2030	pin	35	0.05	10^{-4}
U2031	mqw	47	0.06	5×10^{-4}
U2032	pin	47	0.075	5×10^{-4}

Table 1

Modelled diffusion lengths for ungraded samples at three aluminium fractions. The values of l_n show remarkable consistency at low Al fractions. Poorer consistency at high Al fractions is partly due to variable device performance.

the back surface of the n region.

5.1 Thin p QWSC

More detailed discussion of thin p cells is given in [9]. Preliminary studies indicate that series resistance has a significant effect on unconcentrated AM1.5 performance for thicknesses below about $0.1\mu m$.

5.2 Determination of L_n from Ungraded Devices

The model reproduces the QE of *pin* and QWSC samples with very similar values of L_n and S_n . These are given in table 1. Also shown in the table are the band-gaps extracted from the photocurrent spectra. We note that consistency between different types of samples is very good for $X=20\%$ but deteriorates at higher Al fractions. Theory and QE data for the 30% Al sample are given in figure 2.

Modelling shows that L_n decreases more slowly with increasing Al fraction than has been reported in [6]. It increases near the direct - indirect transition in the region of 40% Al. This trend is consistent with published measurements in the review article [1] although our values are substantially lower for reasons which are not fully understood.

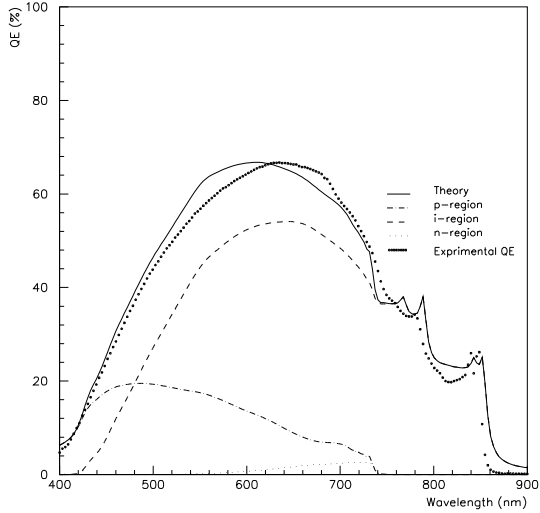


Fig. 2. Experimental data and model for a 33% Al fraction 30 MQW solar cell used to determine values of L_n .

5.3 Determination of $\nabla_X D_n$ from Graded QWSCs

Graded samples were used to establish diffusion constant gradients between the four different Al fractions and are given in table 2. The QE data and theory for the 33% Al graded QWSC U4034 are given in figure 3.

Figure 5 shows the experiment and theory for the mirror backed MOVPE sample QT468a. The integrated J_{sc} enhancement for this device was 49% in the well and of 28% in J_{sc} overall. Fabry-Perot peaks are visible, showing that front and back surface interfaces are smooth. Other samples with accidentally roughened back mirrors have shown higher J_{sc} enhancements. This is attributed to non-specular reflection at the back surface which increases the optical path length in the cell and hence improves light absorption.

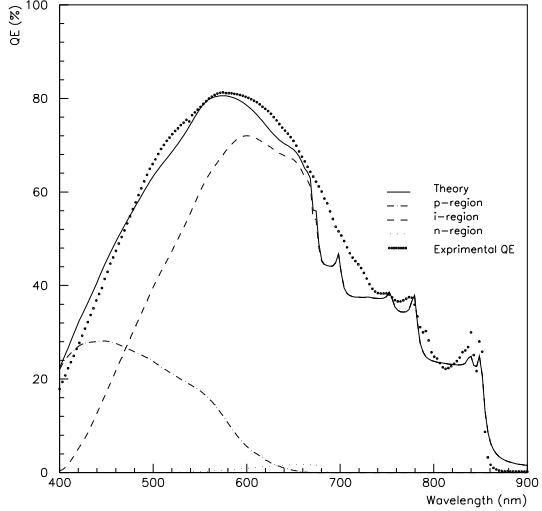


Fig. 3. Experimental data and model for a 33% Al fraction 30 MQW solar cell incorporating a *p* region compositionally graded from 33% to 67% Al. Comparison with figure 2 shows significantly improved QE at short wavelengths.

Sample	<i>p</i> grade		$\nabla_X D_n$ (cm/s)
	Front Al fraction (%)	Back Al fraction (%)	
U4033	22	44	-5.5×10^5
U4034	34	67	-4.5×10^5
U4035	44	67	-4.3×10^5

Table 2

Gradients of the diffusion constant in $\text{Al}_x\text{Ga}_{1-x}\text{As}$ with respect to Al fraction. These values are derived from modelling the QE of graded QWSC samples using the L_n values given in table 1.

6 Results

7 Optimisation

The model was used to design an optimised 50 well QWSC with a thinned and graded *p* layer. We chose to concentrate on a nominal barrier aluminium fraction of 30% and to

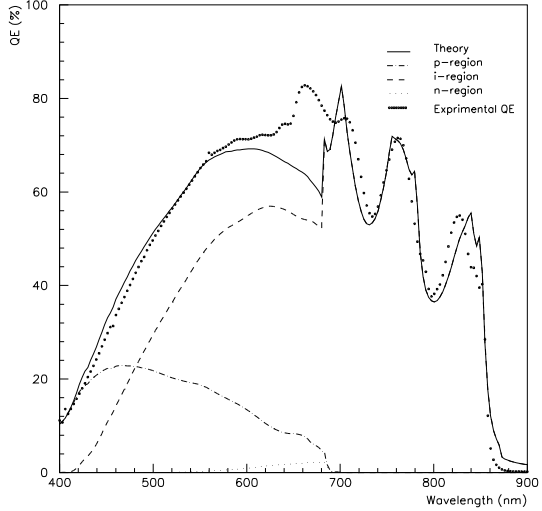


Fig. 4. mirrored 30% cell QT468a showing Fabry-Perot effects. The short circuit current enhancement for this device was 25% overall.

base the design on our best previous G951 cell which is described in [9].

The p layer was thinned to $0.1\mu\text{m}$. Modelling values of J_{sc} predict little current enhancement for grades with a top Al fraction above about 44%. We have therefore limited this optimisation to 44% in view of increasing impurity incorporation at higher Al fractions and greater uncertainty in modelling parameters in this region.

The modelled J_{sc} under standard AM1.5 illumination for a mirror backed device was 27.9 mA cm^{-2} for our contact design which has a 7% shading loss. Comparison with G951 gives us a rough value for the efficiency we expect from this sample. G951 has a V_{oc} of 1.07 V , a fill factor of 78% and a J_{sc} of 17.5 mA cm^{-2} . The V_{oc} is a little low for the optimised cell because of its higher J_{sc} . If, however, we use these parameters to estimate the efficiency of the optimised cell on the basis of the modelled J_{sc} we obtain an efficiency of 22.3%. This compares favourably with a GaAs cell described in [4] which has an efficiency of 25.1% for a fill factor of 87%, a V_{oc} of 1.022 V and a J_{sc} of 28.2 mA cm^{-2} . We note that the QWSC efficiency would improve substantially if the fill factor QWSC were increased.

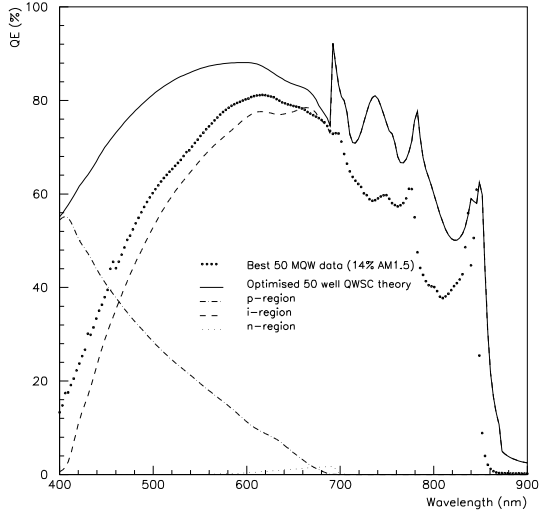


Fig. 5. Optimised 50 well QWSC consisting of a $0.1 \mu\text{m}$ *p* region compositionally graded from 30% - 44% Al and mirror backed. $I_{sc}=25.5\text{mA}(IEC-AM1.5)\text{cm}^{-2}$. Also shown the experiment for the best 30% QWSC prior to optimisation.

8 Conclusion

Previous work has demonstrated current enhancement and promising voltage performance in QWSCs. Further theoretical and experimental investigation has shown that useful J_{sc} enhancements can be made in different wavelength ranges. Improved design of the *p* layer can enhance the disappointing QE of $\text{Al}_x\text{Ga}_{1-x}\text{As}$ cells below 400nm, while a back mirror coating is seen to double the MQW current in 30MQW samples.

Theoretical predictions combining these improvements in a single cell indicate that an $\text{GaAs}/\text{Al}_x\text{Ga}_{1-x}\text{As}$ cell can be grown with efficiencies close to the unconcentrated GaAs cells. Further improvements are expected if fill factors in particular can be increased. The design may be attractive for the high bandgap component of a concentrator system, either as an optimised $\text{Al}_x\text{Ga}_{1-x}\text{As}$ cell, or a QWSC. The QWSC may be attractive for this purpose since its current output can be tuned to that of the lower bandgap component by varying the number and/or width of the quantum wells.

References

- [1] Ahrenkiel R K (1992), Minority – Carrier Lifetime and Diffusion Length in AlGaAs. In: Adachi S (Ed) Properties of Aluminium Gallium Arsenide, EMIS Datareviews Series No. 7, INSPEC, London, pp. 221 – 224.
- [2] Barnham K *et al.* (1994), Quantum well Solar Cells, Optoelectronics – Devices and technologies 9(4), Mita Press, Tokyo, pp. 483 – 498
- [3] Casey H C, Panish B (1978), Heterostructure Lasers, part B. Academic Press, New York
- [4] Green M A *et al.* (1994), Solar Cell efficiency Tables (Version 5), Progress in Photovoltaics 3(1), Wiley:pp 51 – 55
- [5] Haarpaintner G (1994), Voltage Performance of Quantum Well Solar Cells in the $\text{Al}_x\text{Ga}_{1-x}\text{As}/\text{GaAs}$ and the $\text{GaAs}/\text{In}_y\text{Ga}_{1-y}\text{As}$ Material Systems, Proceedings of 1st World Photovoltaic Energy Conference, 5-9 December 1994 Hawaii, pp 1783 – 1786
- [6] Hamaker H C (1985), Computer modelling of the effects of inhomogeneous doping and/or composition in GaAs solar – cell devices, J. Appl. Phys. 58(6):2344 – 2351.
- [7] Hovel H J (1976), Solar Cells. In: Willardson R K, Beer A C (Eds), Semiconductors and Semimetals, Vol. 11, Academic Press New York.
- [8] Hutchby J A (1976), Theoretical Analysis of /gaasalg/ graded band-gap solar cell, J. Appl. Phys 47(7): 3140 – 3151
- [9] Paxman M *et al.* (1993), Modelling the Spectral Response of the Quantum Well Solar Cell, J. Appl. Phys 74(1):614 – 621.
- [10] Roberts J S *et al.* (1994), High Purity AlGaAs from methyl based precursors using in situ gettering of alkoxides, Journal of Crystal Growth 143:135 – 140.
- [11] Singh J (1993), Physics of Semiconductors and their Heterostructures, first edition. McGraw-Hill International Edition.
- [12] Tsui E T *et al.* (1995), Determination of the Quasi fermi level separation in single quantum well p-i-n diodes, submitted to JAP July 1995.

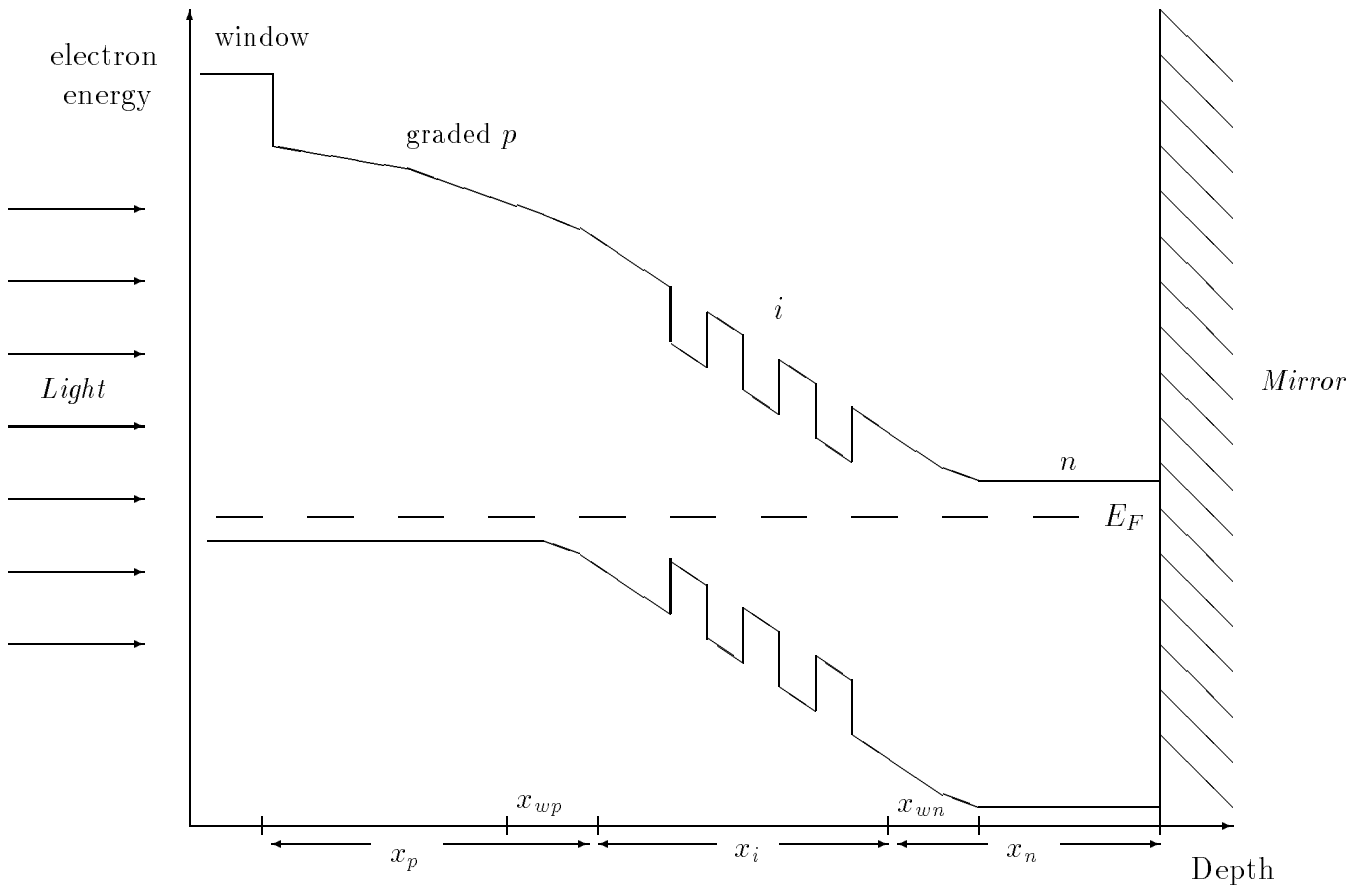


Figure 1 An optimised GaAs/Al_xGa_{1-x}As QWSC

- Quantum wells extend the absorption range to lower wavelengths and increase the photocurrent
- The QWSC shows a higher V_{oc} than expected from a cell made with the quantum well effective bandgap
- Compositional grading of the p layer produces a decreasing bandgap with depth. Efficiency is increased as the bandgap gradient induces carrier to drift towards the junction.
- Compositional grading decreases the p layer optical thickness and allows greater light transmission to the efficient i region
- The wells absorb little light but convert it efficiently. The mirror passes light back through the wells and increases their yield.

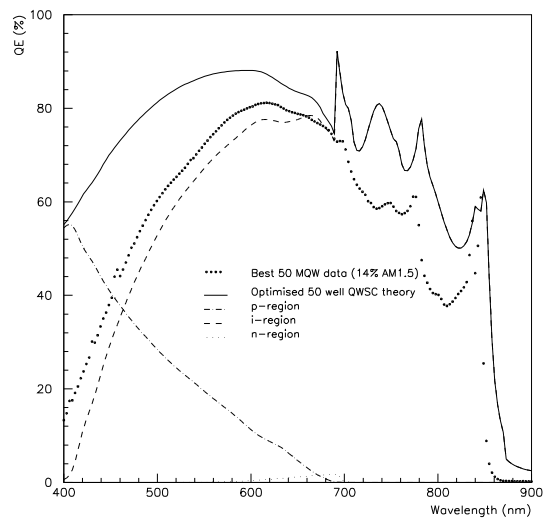


Fig. 5. Optimised 50 well QWSC consisting of a $0.1 \mu\text{m}$ *p* region compositionally graded from 30% to 44% Al and mirror backed. $I_{sc}=25.5 \text{ mA cm}^{-2}$ (IEC AM1.5). Also shown the experiment for the best 30% QWSC prior to optimisation.

References

- [1] Ahrenkiel R K (1992), Minority – Carrier Lifetime and Diffusion Length in AlGaAs. In: Adachi S (Ed) Properties of Aluminium Gallium Arsenide, EMIS Datareviews Series No. 7, INSPEC, London, pp. 221 – 224.
- [2] Barnham K *et al.* (1994), Quantum well Solar Cells, Optoelectronics – Devices and technologies 9(4), Mita Press, Tokyo, pp. 483 – 498
- [3] Casey H C, Panish B (1978), Heterostructure Lasers, part B. Academic Press, New York
- [4] Green M A *et al.* (1994), Solar Cell efficiency Tables (Version 5), Progress in Photovoltaics 3(1), Wiley:pp 51 – 55
- [5] Haarpaintner G (1994), Voltage Performance of Quantum Well Solar Cells in the $\text{Al}_x\text{Ga}_{1-x}\text{As}/\text{GaAs}$ and the $\text{GaAs}/\text{In}_y\text{Ga}_{1-y}\text{As}$ Material Systems, Proceedings of 1st World Photovoltaic Energy Conference, 5-9 December 1994 Hawaii, pp 1783 – 1786
- [6] Hamaker H C (1985), Computer modelling of the effects of inhomogeneous doping and/or composition in GaAs solar – cell devices, J. Appl. Phys. 58(6):2344 – 2351.
- [7] Hovel H J (1976), Solar Cells. In: Willardson R K, Beer A C (Eds), Semiconductors and Semimetals, Vol. 11, Academic Press New York.
- [8] Hutchby J A (1976), Theoretical Analysis of /gaasalg/ graded band-gap solar cell, J. Appl. Phys 47(7): 3140 – 3151
- [9] Paxman M *et al.* (1993), Modelling the Spectral Response of the Quantum Well Solar Cell, J. Appl. Phys 74(1):614 – 621.
- [10] Roberts J S *et al.* (1994), High Purity AlGaAs from methyl based precursors using in situ gettering of alkoxides, Journal of Crystal Growth 143:135 – 140.
- [11] Singh J (1993), Physics of Semiconductors and their Heterostructures, first edition. McGraw-Hill International Edition.
- [12] Tsui E T *et al.* (1995), Determination of the Quasi fermi level separation in single quantum well p-i-n diodes, submitted to JAP July 1995.

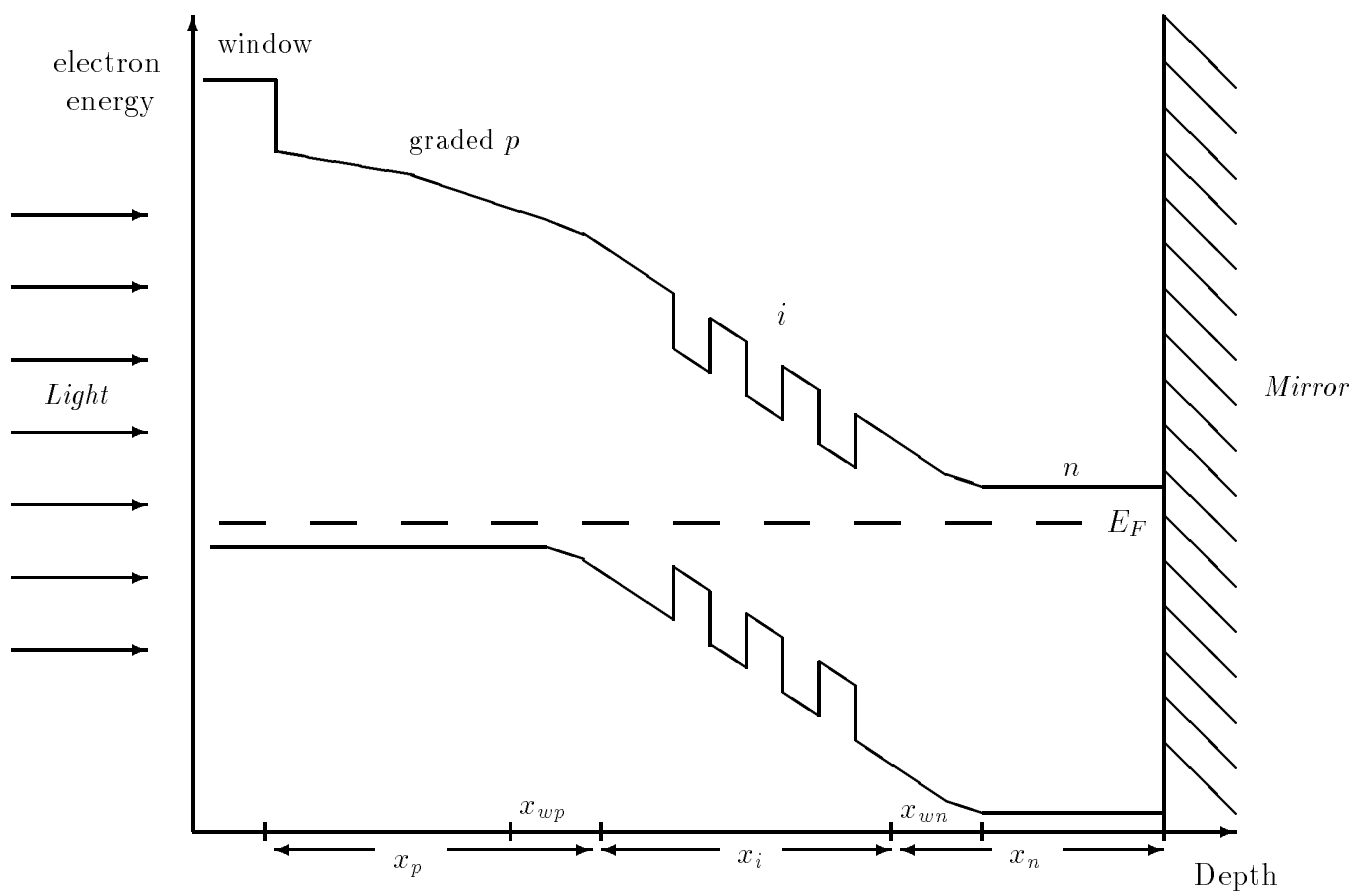


Figure 1. QWSC band diagram

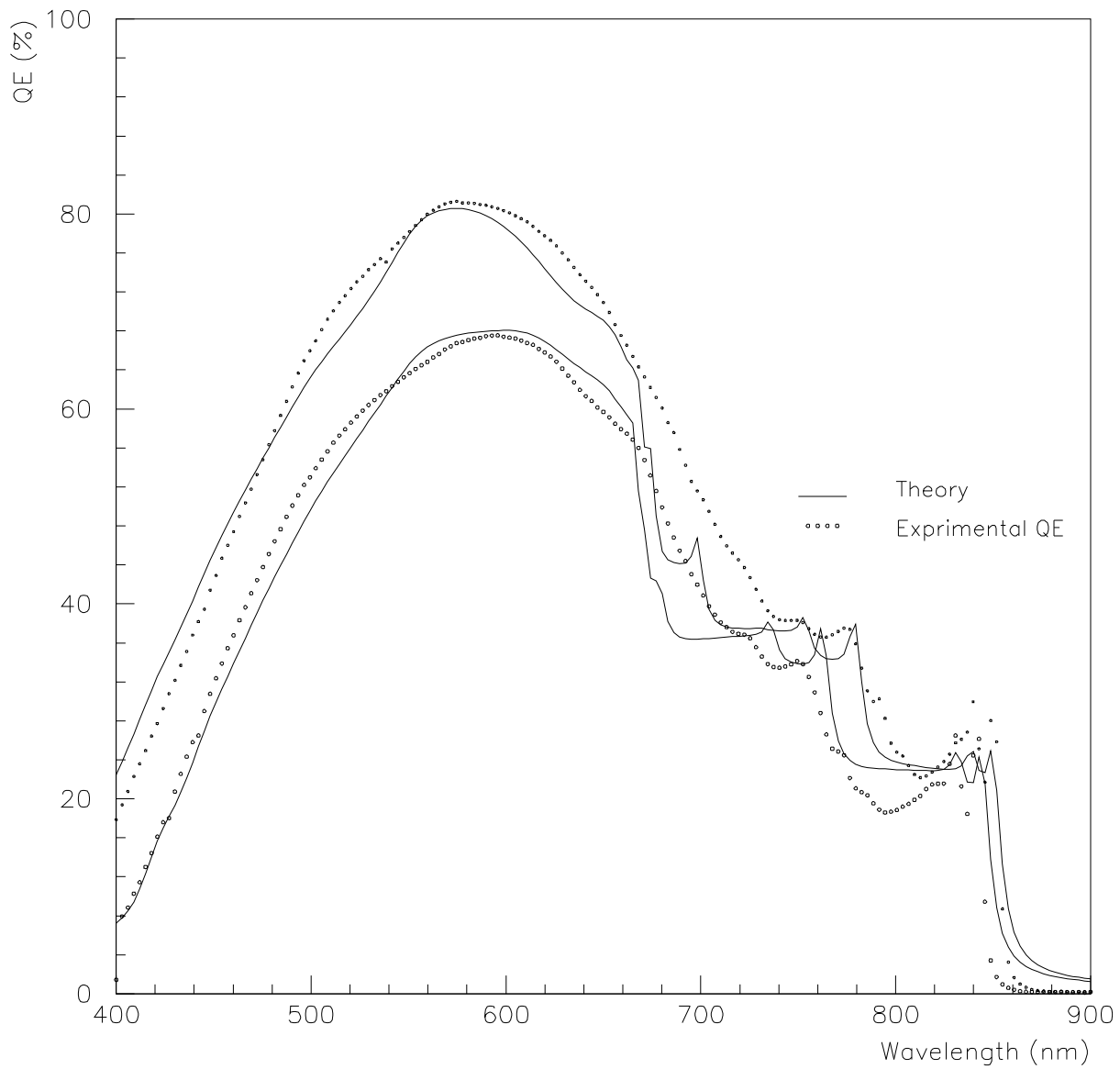


Figure 2. A QWSC with a graded p layer (upper curve) shows a substantially improved short wavelength quantum efficiency compared to an ungraded but otherwise identical 30 well QWSC (lower curve).

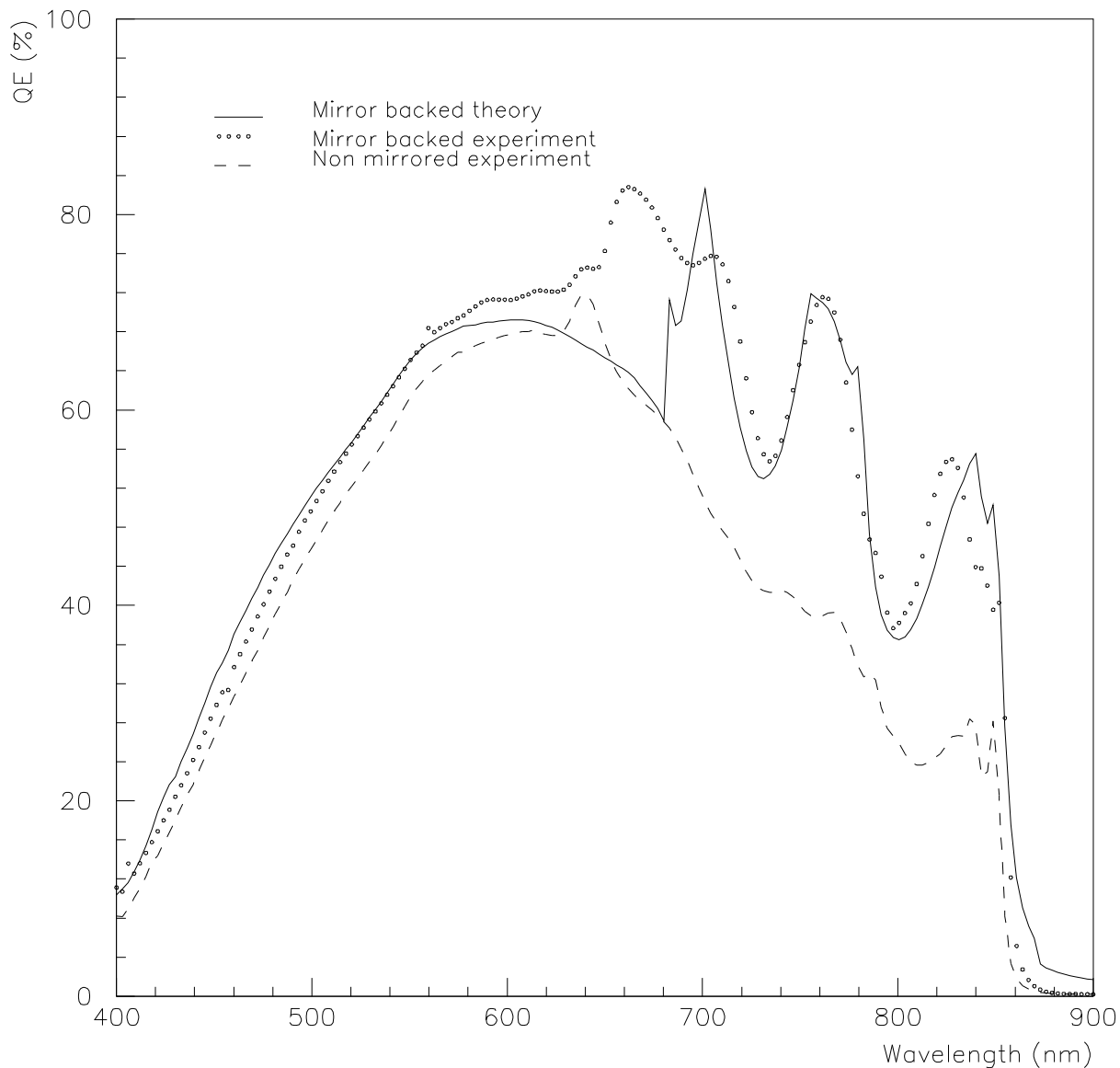


Figure 3. A mirror backed QWSC shows a significantly increased current contribution from the quantum wells. This technique is particularly well suited to QWSCs because the wells absorb relatively little light on the first pass.

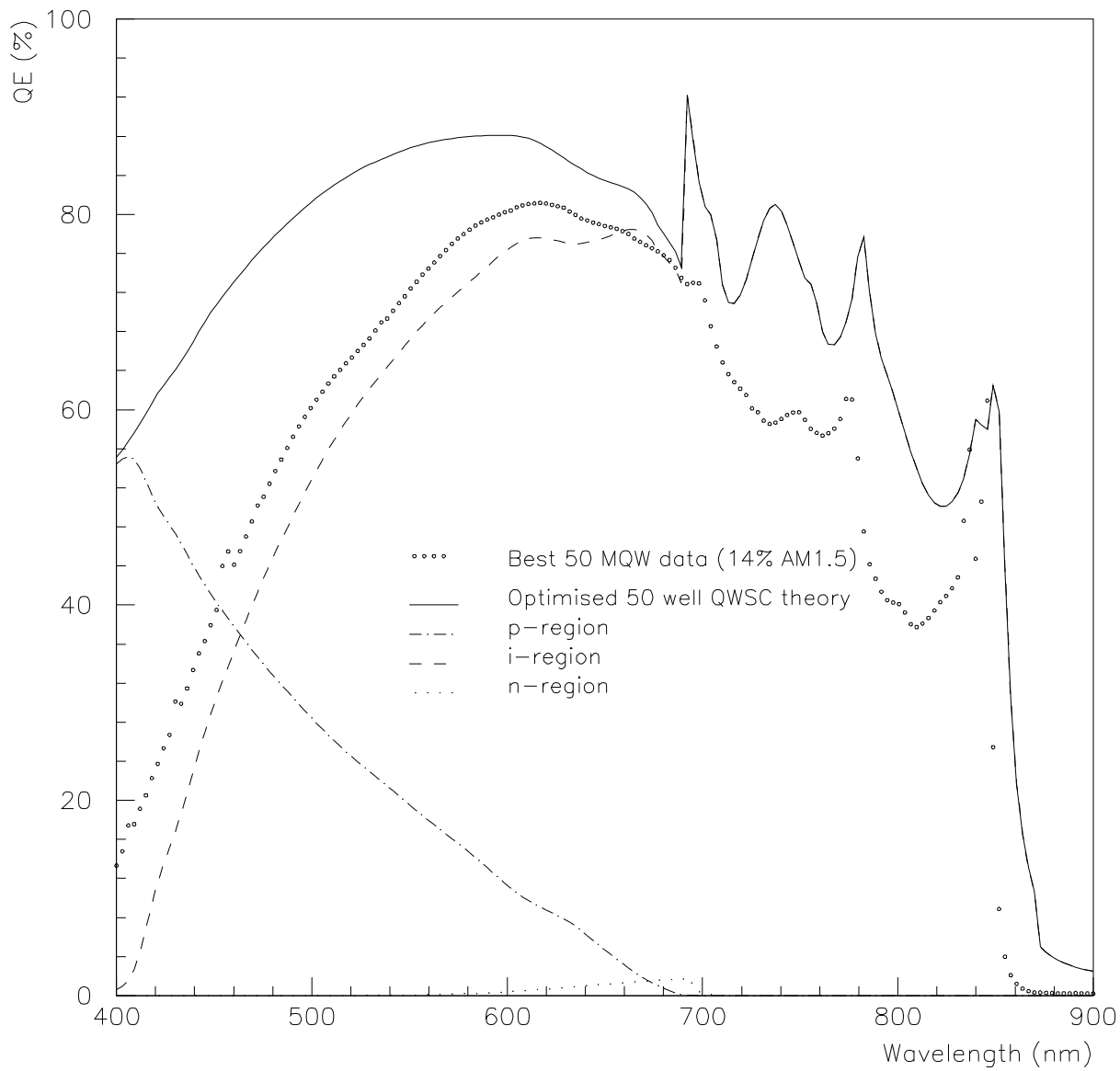


Figure 4. Optimised 50 well QWSC with a $0.1\mu\text{m}$ p layer compositionally graded from 30% to 44% aluminium and coated with a mirror. Also shown is the experiment for the previous best 14% efficient 30 well QWSC.